Influence of Polyelectrolyte Multilayer Films on Calcium Phosphate Nucleation

P. A. Ngankam,[†,§] Ph. Lavalle,[‡] J. C. Voegel,*[,†] L. Szyk,[†] G. Decher,[§] P. Schaaf,[§] and F. J. G. Cuisinier[†]

Contribution from the Fédération de Recherches "Odontologie" U424 INSERM, Université Louis Pasteur (ULP), 11, rue Humann, 67085 Strasbourg Cedex, France, Biozentrum, Department of Biophysical Chemistry, 4056 Basel, Switzerland, and Institut Charles Sadron (CNRS-ULP), 6, rue Boussingault, 67083 Strasbourg Cedex, France.

Received March 3, 2000

Abstract: The nucleation of calcium phosphate crystals from a weakly supersaturated calcium phosphate solution on the surface of polyelectrolyte multilayers was investigated in dependence on the chemical nature of the outermost layer. Scanning angle reflectometry was used to follow in situ the initial stages of the nucleation kinetics. The multilayers were constructed by alternate adsorption of poly(styrene sulfonate) (PSS) and poly(allylamine) (PAH), leading to oppositely charged surfaces. It was verified that films terminating with either PSS or PAH exhibited a negative or positive ζ-potential, respectively. Surprisingly, both types of surface layers induced a nucleation process for supersaturations smaller than the one observed on the bare silica surface. According to the literature, such an effect should only be expected on a negatively charged surface. Infrared spectroscopy showed that the nucleated crystals are hydroxyapatite (OHAP) or octacalcium phosphate (OCP) but not dicalcium phosphate dihydrate (DCDP) which is found on bare silica surfaces. On both PSS and PAH surfaces, the nucleation processes started only after a given induction time. The evolution of the induction times with different supersaturations was analyzed within the framework of the classical nucleation theory. The effective surface free energies of the formed crystals were estimated to be on the order of 32 $mJ \cdot m^{-2}$ on a multilayer terminating with PSS and to be about 37 $mJ \cdot m^{-2}$ on a multilayer terminating with PAH. A mechanism for the enhanced nucleating effect of such polyelectrolyte surfaces is proposed.

Introduction

Biomineralization[1,2] is a general process by which inorganic salt crystals (frequently calcium carbonate or calcium phosphate) are produced in biological environments. As an example one can take the ordered deposition of calcium phosphate salts on an extracellular organic matrix by means of a heterogeneous nucleation process, which constitutes the first stage of hard tissue mineralization in all vertebrae.[3,4] Although the process is of tremendous importance for life as we know it, little is known about the details that control biomineralization at the molecular level. As a consequence, it is of high interest to study certain aspects of biomineralization by exact physical methods. It is therefore necessary to study mineralization in artificial systems that allow the chemical nature of the nucleation sites to be modified in a controlled way and that allow at the same time data on nucleation kinetics and on the structure of the crystals formed to be obtained. A convenient system for physical characterization is to induce mineralization on solid surfaces, whose chemical nature is easily controlled by physisorption or chemisorption.

Biomimetic properties of such films would consist in promoting only heterogeneous nucleation within the film at quite low bulk concentrations so that homogeneous nucleation in solution is completely avoided. At the same time, polyelectrolyte surfaces should also promote adhesion of the inorganic salt crystals formed at the interface. For example, Zhang and Gonsalves[5] promoted the heterogeneous nucleation of calcium carbonates crystals on poly(acrylic acid) adsorbed onto chitosan surfaces. The influence of polyelectrolytes onto crystallization has been widely investigated,[6,7] and they either favor nucleation after their uptake onto a sorbent surface or inhibit the process after their adsorption onto the crystal surface. Multilayers resulting from alternated adsorption of anionic and cationic polyelectrolytes constitute another original way of preparation of functionalized films with control of surface charge.[8] An additional benefit from polymer-treated interfaces is that polymer segments extend about 1 nm into the adjacent liquid and that they are soft and can therefore adapt to the surface of the nucleating crystal.

The aim of the present study is to investigate the influence of polyelectrolyte films using poly(allylamine) (PAH) as cationic and poly(styrenesulfonate) (PSS) as anionic polyelectrolytes onto calcium phosphate mineralization. These polymers were chosen

* To whom correspondence should be addressed. Telephone: (33) 3 88 24 33 95. Fax: (33) 3 88 24 33 99. E-mail: jcv@odont3.u-strasbg.fr.
† U424 INSERM.
‡ Biozentrum.
§ Institut Charles Sadron.

(1) Heywood, B. R.; Mann, S. *Adv. Mater.* **1994**, *1*, 9.
(2) Weiner, S.; Traub, W. *Philos. Trans. R. Soc. London* **1984**, *B 304*, 425.
(3) Hunter, G. K.; Goldberg, H. A. *Proc. Natl. Acad. Sci. U.S.A.* **1993**, *18*, 8562.
(4) Cuisinier, F. J. G.; Steuer, P.; Brisson, A.; Voegel, J. C. *J. Cryst. Growth* **1995**, *156*, 443.
(5) Zhang, S.; Gonsalves, K. E. *Langmuir* **1998**, *14*, 6761.
(6) Dalas, E.; Kallitsis, J. K.; Koustoukos, P. G. *Langmuir* **1991**, *7*, 1822.
(7) Marentette, J. M.; Norwig, J.; Stöckelmann, E.; Meyer, W. H.; Wegner, G. *Adv. Mater.* **1997**, *9*, 647.
(8) Decher, G. *Science* **1997**, *277*, 1232.

10.1021/ja000783o CCC: $19.00
Published on Web 09/01/2000

because their deposition in multilayer films is well studied; variations of the chemical nature of the polyelectrolytes will be an option for future studies. Mineralization was followed "in situ" using scanning angle reflectometry (SAR). This technique constitutes an excellent tool, allowing a precise determination of the critical supersaturation, of induction time, and of structural properties such as layer thickness.[9] The deposited crystals were further investigated by means of scanning electron microscopy (SEM) to determine crystal morphology and by infrared (IR) spectroscopy in order to characterize the chemical nature of the crystals.

Materials and Methods

Chemicals. Experiments were performed using calcium and phosphate solutions. Calcium solutions were prepared from $CaCl_2$ (purity 99.5%) (Merck). Phosphate solutions were obtained by mixing equimolar solutions of $Na_2HPO_4 \cdot 7H_2O$ and $NaH_2PO_4 \cdot H_2O$ (purity 98.5%)-(Merck). Trishydroxy-aminomethane (Tris, purity 99.9%) was purchased from Sigma. Equimolar calcium/phosphate solutions (Ca/P = 1) were prepared with Tris/HCl buffer in the presence of 150 mM NaCl. The final pH of the solutions was 6.85 ± 0.05.

Anionic poly(sodium 4-styrenesulfonate) (PSS, MW = 70000 g/mol), cationic poly(allylamine hydrochloride) (PAH, MW = 50000−65000 g/mol) and cationic poly(ethyleneimine) (PEI, MW = 75000 g/mol), were purchased from Aldrich. Solutions of PSS and PAH were prepared by dissolving the polyelectrolytes in 10 mM Tris/HCl buffer (150 mM NaCl) at pH 7.4. The final concentration of these solutions was 5 $mg \cdot ml^{-1}$. The PEI solutions were prepared by dissolving 500 mg of PEI in 100 mL of pure water. All solutions were prepared with ultrapure deionized water (Millipore Corporation).

Scanning Angle Reflectometry. The polyelectrolyte deposition and the calcium/phosphate mineralization processes were followed in situ by using SAR. This optical technique allows, in principle, to get access to the optical thickness and the refractive index of a film deposited on an optically flat surface. The scanning angle reflectometer and the experimental details have been described in previous publications.[9,10] Briefly, the technique is based on the variations, after adsorption, of the reflection coefficient of an electromagnetic wave polarized in the plane of incidence (p-wave), the incidence angle being close to the Brewster angle (θ_B). At the Brewster angle, the reflectivity of a p-wave is null for a perfectly abrupt, planar interface (Fresnel interface). Once a film is deposited on such a surface, not only does the reflected intensity at the Brewster angle differ from zero, but the whole reflectivity curve (reflected intensity as a function of incidence angle) can change in shape and position. From these variations one extracts information about the deposited film.

The reflectometer is composed of a 5 mW HeNe laser (Melles Griot, Irvine, CA, USA) producing almost linearly polarized light ($\lambda = 632.8$ nm). This light passes through a Suprasyl prism to reflect on the inner, optically polished surface ($\lambda/4$) supporting the deposited film under investigation. This surface forms one face of the experimental cell. Before and after reflection, the beam passes through two polarizers which select the p-polarization and which achieve a polarization ratio greater than 10^7. The incidence angle is selected with an angular precision of $\pm 0.005°$. The reflected intensity is recorded at various incidence angles around θ_B. The measurements are performed during the deposition of the polyelectrolytes and after the addition of calcium and phosphate solutions in the cell. The recorded reflectivity curves are then analyzed. One usually uses the homogeneous isotropic layer model.[11] Within this model the layer is characterized by the mean refractive index increment Δn (the difference between the refractive index of the layer and of the solution) and by an optical thickness L. The total adsorbed quantity is assumed to be proportional to the product $\Delta n \cdot L$. The parameters L and Δn are determined by a nonlinear least-squares regression fitting procedure.[12] The quality of the fitting procedure is evaluated by mean of the least-squares parameter χ^2.

$$\chi^2 = \frac{1}{N}\sum_{i=1}^{N}\left(\frac{I_{exp}(\theta_i) - I_{th}(\theta i,\Delta n,L)}{0.01 I_{exp}(\theta i) + \sigma_0}\right)^2 \quad (1)$$

with θ_i the incidence angle, N the number of angles at which measurements were performed and σ_0 corresponds to the background noise. $I_{exp}(\theta_i)$ and $I_{th}(\theta_i,\Delta n,L)$ correspond to the experimental and theoretical reflected intensities.[11]

Typical SAR Experiments. Each experiment was preceded by an extensive purification of cell and tubing with a cleaning solution (Hellmanex, 2% in water, Hellma, Mullheim, Germany) by heating to 50 °C for 10 min. A 2 min rinse with HCl (1%) and a further extensive rinse with deionized water followed. Then, a first reference reflectivity curve was determined in the presence of pure water. The build-up of the polyelectrolyte film was performed by sequential injections of cationic and anionic polyelectrolyte solutions with extensive rinses between consecutive deposition steps. The first layer on the prism always consisted of PEI adsorbed for 30 min. After rinsing with 250 mL of H_2O, the PSS solution was injected and maintained in contact with the surface for 15 min. Again, the cell was rinsed with 150 mL of H_2O, followed by a 50 mLTris/HCl rinse. The architecture of the film, composed of two layers at this point, will be denoted as PEI−PSS. Adsorption of the next (PAH) layer leads to the film architecture PEI−PSS−PAH. The final film architectures PEI−$(PSS-PAH)_2$ and PEI−$(PSS-PAH)_2$−PSS were obtained after carrying out the respective numbers of adsorption cycles.

Calcium/Phosphate Crystal Nucleation Process Followed by SAR. After the formation of the polyelectrolyte multilayer, the experimental cell was emptied and directly brought in contact with the calcium/phosphate solution. Great care was taken to keep the surface wet during the whole operation. The crystal nucleation process was then followed by SAR, the calcium/phosphate solution remaining at rest in the cell. It should be pointed out that in SAR one is only sensitive to refractive index changes on the reflecting surface and not in the bulk solution (as long as the refractive index of the supersaturated solution does not change significantly). Even more, if bulk nucleation would take place, the crystals formed in this way would sediment toward the bottom of the cell and would not deposit on the reflecting surface which is in a vertical position. The changes in the reflectivity curves are thus entirely due to changes of the optical characteristics of the reflecting surface.

The polyelectrolyte film build-up and the mineralization process were followed by determining a reflectivity curve every 10 min. A signal corresponding to the onset of nucleation on the multilayer manifests itself as an increase of the reflectivity around the Brewster angle θ_B.

A typical experiment lasted for 25 h, the first 5 h corresponding to the building up of the polyelectrolyte film followed by other 20 h which corresponded to the mineralization step. The reproducibility was checked by performing each experiment at least twice.

Characterization of the Deposited Material. SAR results were complemented with the aid of several techniques in order to obtain data on morphology and structural properties of the deposited crystals. SEM was used for the morphology investigations. The structural characterization of the deposited material was carried out by IR spectroscopy. This was done by performing two experiments in parallel: one directly in the reflectometer and the second one in a cell composed of the same material as that of the prism (Suprasyl) and polished optically in the same way by the same manufacturer (Thuet Biechlin, Blodelsheim, France). Both experiments were started simultaneously with identical calcium and phosphate solutions. After a given reaction time as estimated from the evolution of the reflectivity curves, the silica slides of the second cell were immediately rinsed with ultrapure deionized water and air-dried to stop further nucleation and growth. Specimen were then specifically prepared for SEM and IR analyses. For SEM investigations slides were coated with gold−palladium in a Hummer junior evaporator (Siemens, Karlsruhe,

(9) Ngankam, A. P.; Schaaf, P.; Voegel, J. C.; Cuisinier, F. J. G. *J. Cryst. Growth* **1999**, *197*, 927.

(10) Schaaf, P.; Dejardin, Ph.; Schmitt. A. *Langmuir* **1987**, *3*, 1131.

(11) Heinrich, L.; Mann, E. K.; Voegel, J. C.; Koper, G. J. M.; Schaaf, P. *Langmuir* **1996**, *12*, 4857.

(12) Press, W. H.; Flannery, B. P.; Teukolsky, S. A.; Vetterling, W. T. *Numerical Recipes In Pascal, The Art of Scientific Computing*; Cambridge University Press: New York, 1990; p 326.

Table 1. Thicknesses (L), Refractive Index Increments (Δn), and the Total Quantities ($\Delta n \cdot L$) Observed after the Deposition of PEI−(PSS−PAH)$_2$−PSS and PEI−(PSS−PAH)$_2$ Polyelectrolyte Films[a]

	PEI−(PSS−PAH)$_2$−PSS	PEI−(PSS−PAH)$_2$
number of experiments	5	16
L(nm)	16.3± 2.5	17.2 ± 6.7
Δn	0.150 ± 0.001	0.150 ± 0.001
$\Delta n \cdot L$ (nm)	2.4 ± 0.4	2.6 ± 1

[a] The second line of the table corresponds to the number of independent experiments performed for each film. For each film, both L and $\Delta n = n_{lay} - n_{sol}$ were determined independently, n_{lay} representing the refractive index of the layer and n_{sol} the refractive index of the solution. The values presented correspond to the mean values and the given uncertainties of the standard deviations.

Germany), and analyzed using a SEM Stereoscan, (Cambridge, UK) operating at 35 kV. IR Spectroscopy experiments were performed with an EQUINOX 55 apparatus (Bruker, Karlsruhe, Germany) in reflectance mode. The data of crystals formed by interfacial nucleation were compared with transmittance spectra of dicalcium phosphate dihydrate (DCPD), octacalcium phosphate (OCP), and hydroxyapatite (OHAP) monitored on the same apparatus and with reference spectra of PEI−(PSS−PAH)$_2$ and PEI−(PSS−PAH)$_2$−PSS multilayer films adsorbed onto silica slides.

Results and Discussion

The build-up of the polyelectrolyte multilayers was followed at first by SAR. The final thickness (L), the refractive index increment (Δn) and the value of ($\Delta n \cdot L$), reached after deposition of PEI−(PSS−PAH)$_2$−PSS and PEI−(PSS−PAH)$_2$ are given in Table 1. The large relative uncertainties given for the different thicknesses are partly due to the small differences which were measured between the reflectivity curves relative to the polyelectrolyte multilayers and the Fresnel curve. The values reported in Table 1 are, nevertheless, comparable to those found in a previous study for similar polyelectrolyte multilayers.[13] Independently, zeta-potential (ζ-potential) measurements were performed on similar multilayers deposited on silica capillaries to control the sign of charge of multilayer films of different architecture. The experimental method and the experimental conditions were described in details in reference.[13] The multilayers with an outer PSS layer showed a ζ-potential of -90 ± 10 mV. The surface became positively charged when PAH was deposited as outer layer with a ζ-potential equal to $+65 \pm 5$ mV. In comparison, the bare silica surface of the capillary was characterized by a ζ-potential of about -110 mV.

In the next step the reflectivity curves of multilayer films in contact with calcium/phosphate solutions were recorded. The calcium/phosphate concentrations were varied from 4.5 to 6.75 mM for PEI−(PSS−PAH)$_2$ and from 5.0 to 7.75 mM for PEI−(PSS−PAH)$_2$−PSS. A typical evolution of such reflectivity curves with contact time between a PEI−(PSS−PAH)$_2$−PSS (respectively PEI−(PSS−PAH)$_2$) multilayers and the calcium/phosphate solution is shown in Figure 1a (respectively 1b). The corresponding time evolutions of the reflected intensities at a given incidence angle are also represented in Figure 2a (respectively 2b) and can be compared (Figure 2c) with the intensities found with the bare prism surface (9). It comes out that during the 20 h of experiments, reflectivity changes are only observed when the calcium/phosphate concentration of the solution in contact with the surface exceeds a certain critical value (C_c). This critical concentration is found to be equal to 5.38 ± 0.36 mM for PEI−(PSS−PAH)$_2$−PSS multilayer, and

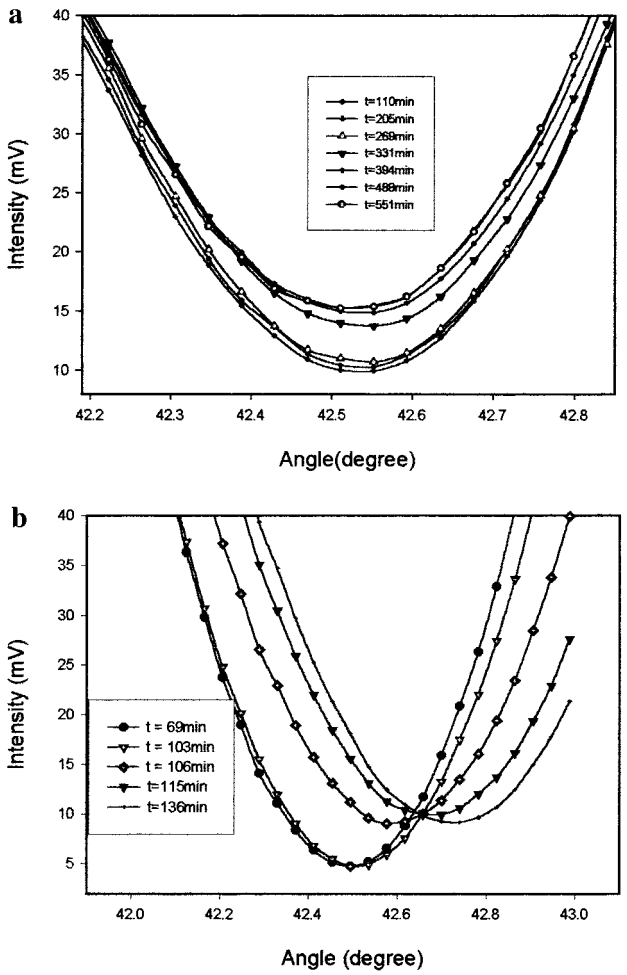

Figure 1. (a) Reflectivity curves in the presence of a calcium/phosphate solution at a concentration of 6.12 mM for different contact times between the solution and the PEI−(PSS−PAH)$_2$−PSS film. The different time scales at which the reflectivity curves were determined are given in the inset. (b) Reflectivity curves in the presence of a calcium/phosphate solution at a concentration of 6.75 mM for different contact times between the solution and the PEI−(PSS−PAH)$_2$ film. The different times at which the reflectivity curves were determined are given in the inset.

5.94 ± 0.19 mM for PEI−(PSS−PAH)$_2$ (Table 2). Surprisingly, both anionic and cationic surfaces lead to a C_c significantly lower than the value of 7.6 ± 0.05 mM observed for the nucleation on the bare surface of the prism (Suprasyl).[9] One can thus point out that not only negatively charged surfaces (PEI−(PSS−PAH)$_2$−PSS) strongly induce the nucleation process, but also positively charged surfaces such as PEI−(PSS−PAH)$_2$.

When the multilayers are brought in contact with the supersaturated calcium/phosphate solution above the critical concentration, the nucleation process does not start instantaneously, but changes in the reflectivity curves are only visible after a given induction time. This induction time depends on the calcium/phosphate solution concentration, and the measured values are reported in Table 3. As expected, induction times increase when the solution concentration is decreased.

SEM was used to visualize the crystals, which were formed on the multilayer surfaces. Typical images of surfaces coated with PEI−(PSS−PAH)$_2$−PSS and PEI−(PSS−PAH)$_2$ which were in contact with a 6.75 mM calcium/phosphate solution are shown in Figure 3a and b. On both images platelike crystals are present which can be compared (Figure 3c) with the

(13) Ladam, G.; Schaad, Ph.; Voegel, J. C.; Schaaf, P.; Decher, G.; Cuisinier, F. *Langmuir* **2000**, *16*, 1244.

Table 2. Critical Calcium Supersaturation Values (Second Line) Determined Experimentally for PEI−(PSS−PAH)$_2$−PSS and PEI−(PSS−PAH)$_2$, and the Bare Silica Surfaces[a]

	PEI−(PSS−PAH)$_2$−PSS	PEI−(PSS−PAH)$_2$	bare silica
critical calcium/phosphate concentrations	5.38 ± 0.36 mM	5.94 ± 0.19 mM	7.60 ± 0.15 mM
relative supersaturations (relative to OHAP)	20 ± 1	21 ± 1	27 ± 1
pH values corresponding to critical calcium concentrations for the three calcium/phosphate salts			
OHAP	4.82	4.77	4.64
DCPD	5.79	5.70	5.44
OCP	5.75	5.57	5.53

[a] The relative supersaturations (third line) were estimated from relation 5. Saturating pH values for OHAP (line 5) for DCDP (line 6) and for OCP (line 7) were obtained from the values of line 2 and relations (2−4) by replacing IP by the corresponding K_{SP} values (see also Appendix).

crystallites found in the presence of bare silica put in contact with a 7.62 mM calcium/phosphate solution. The surface coverage appears to be more homogeneous in the case of PEI−(PSS−PAH)$_2$ (typical crystal size of the order of 1−3 μm), than for the PEI−(PSS−PAH)$_2$−PSS surface where dispersed crystallite islands are observed. In this later case the characteristic size of the deposited crystals is on the order of 10 μm. These characteristic sizes were roughly evaluated from the horizontal widths determined from SEM. For comparison, on a silica surface the deposited layer appeared by the aid of SEM observations to be constituted by crystals having platelike habits and were not densely packed.

We fitted the reflectivity curves obtained by SAR by using the model of an homogeneous and isotropic monolayer characterized by the refractive index increment and an optical thickness. In the case of the nucleation process taking place on a PEI−(PSS−PAH)$_2$ surface we could only analyze the first 200 min of the nucleation process. Indeed, the whole reflectivity curves not only changed in shape during the process, but they also strongly shifted so that the minimum of the curves moved out of the range of angles over which the reflected intensities were measured. In Figure 4 we show the evolution of the optical thickness and of the refractive index increment for a nucleation process taking place on a PEI−(PSS−PAH)$_2$ multilayer for the period of time during which the analysis was possible, the concentration of the solution being equal to 6.75 mM. This result was thus obtained under the same conditions as the ones corresponding to the SEM image represented on Figure 3b. It comes out that, at this concentration, the layer seems to reach very rapidly its final thickness. The measured optical thickness of 3.7 μm is not incompatible with the typical crystal dimensions measured on Figure 3b. This is in agreement with the results previously obtained,[9] where the optical thickness of the crystal layer determined from similar SAR experiments was in full agreement with the crystal layer thickness measured by transmission electron microscopy. In Table 3 we give the values of the optical thicknesses measured on PEI−(PSS−PAH)$_2$−PSS and PEI−(PSS−PAH)$_2$ multilayers for different calcium/phosphate concentrations for the latest reflectivity curve which could be analyzed. It comes out that for PEI−(PSS−PAH)$_2$−PSS the thicknesses are much smaller than the ones obtained on PEI−(PSS−PAH)$_2$. However, these values seem incompatible with the SEM observations. The possible explanation is that the surface is constituted by an assembly of widely separated crystal islands of typical size of 5−10 μm (see Figure 3b), which are thus much larger than the wavelength of light. The homogeneous and isotropic monolayer model would thus no longer constitute a good approximation. These results show that optical techniques should never be used solely to analyze quantitatively layers originating from crystal nucleation processes but one should always use a complementary technique such as electron microscopy to ensure the validity of the results. However, scanning angle reflectometry still allows, in the case of the nucleation process on polyelectrolyte multilayers, to get access, in situ, to the pertinent information constituted by the induction time and the critical nucleation concentration.

To obtain information about the nature of the crystals formed at the interface we performed IR spectroscopy. The IR spectra for hydroxyapatite (OHAP), dicalcium phosphate (DCPD), and octacalcium phosphate (OCP) and of the calcium phosphate salts deposited onto PEI−(PSS−PAH)$_2$−PSS and on PEI−(PSS−PAH)$_2$ films are given in Figure 5. The principal vibration bands are gathered in Table 4. It can first be noticed that the spectra obtained on PEI−(PSS−PAH)$_2$ and PEI−(PSS−PAH)$_2$−PSS exhibit very similar vibration bands indicating that the same crystals seem to form on both surfaces. The three main vibration bands found at 1018, between 593 and 598, and around 551 cm^{-1} correspond well with some major bands of OHAP at 1014 cm^{-1} (anti-symmetric P−O elongation of PO_4^{3-}), 597 cm^{-1} (anti-symmetric deformation of PO_4^{3-} and HPO_4^{2-}) and 552 cm^{-1}. The vibrations around 1035 and at 954, 594, 552, and 523 cm^{-1} could also constitute a signature for the presence (or remaining) of OCP. Comparatively, IR spectra of polyelectrolytes without any deposited calcium/phosphate salts gave no vibration bands around 1018 cm^{-1} (data not shown).

Moreover, on our samples, crystal layers were more than 10 times thicker than the polyelectrolyte layer, so that one can safely assume that the transmittance originates mainly from the larger mass fraction of the sample which is constituted by calcium/phosphate deposits. Comparison between these spectra and the spectrum of DCPD allows clearly to conclude that, in contrary to what has been found on a bare silica surface, there is no DCPD phase formed in the presence of both types of multilayers.

From the values of the critical calcium/phosphate concentrations given in Table 3, and by assuming a Ca/P ratio of 1, one can derive the ionic products (IP) for OHAP, DCPD, and OCP as:

$$IP_{OHAP} = f_{Ca^{2+}}^{5} f_{PO_4^{3-}}^{3} [Ca^{2+}]^8 F^3(PO_4^{3-}) \frac{K_w}{f_{H^+}[H^+]} \quad (2)$$

$$IP_{DCPD} = f_{Ca^{2+}} f_{HPO_4^{2-}} [Ca^{2+}]^2 F(HPO_4^{2-}) \quad (3)$$

$$IP_{OCP} = f_{Ca^{2+}}^{4} f_{PO_4^{3-}}^{3} [Ca^{2+}]^7 F^3(PO_4^{3-}) \quad (4)$$

where $f_{Ca^{2+}}$, $f_{PO_4^{3-}}$, $f_{HPO_4^{2-}}$, f_{H^+} represent respectively the activity factors of Ca^{2+}, PO_4^{3-}, HPO_4^{2-}, H^+. K_w, corresponds to the ionic product of water (1.01 10^{-14} at 25 °C), and $F(PO_4^{3-})$ (respectively $F(HPO_4^{2-})$) are the phosphate fraction present in the form of PO_4^{3-} (respectively HPO_4^{2-}). These fractions are pH dependent and were estimated from the three different phosphate equilibria.[14−16] The activity coefficients were esti-

(14) Nims, L. F. *J. Am. Chem.* **1934**, *56*, 1110.

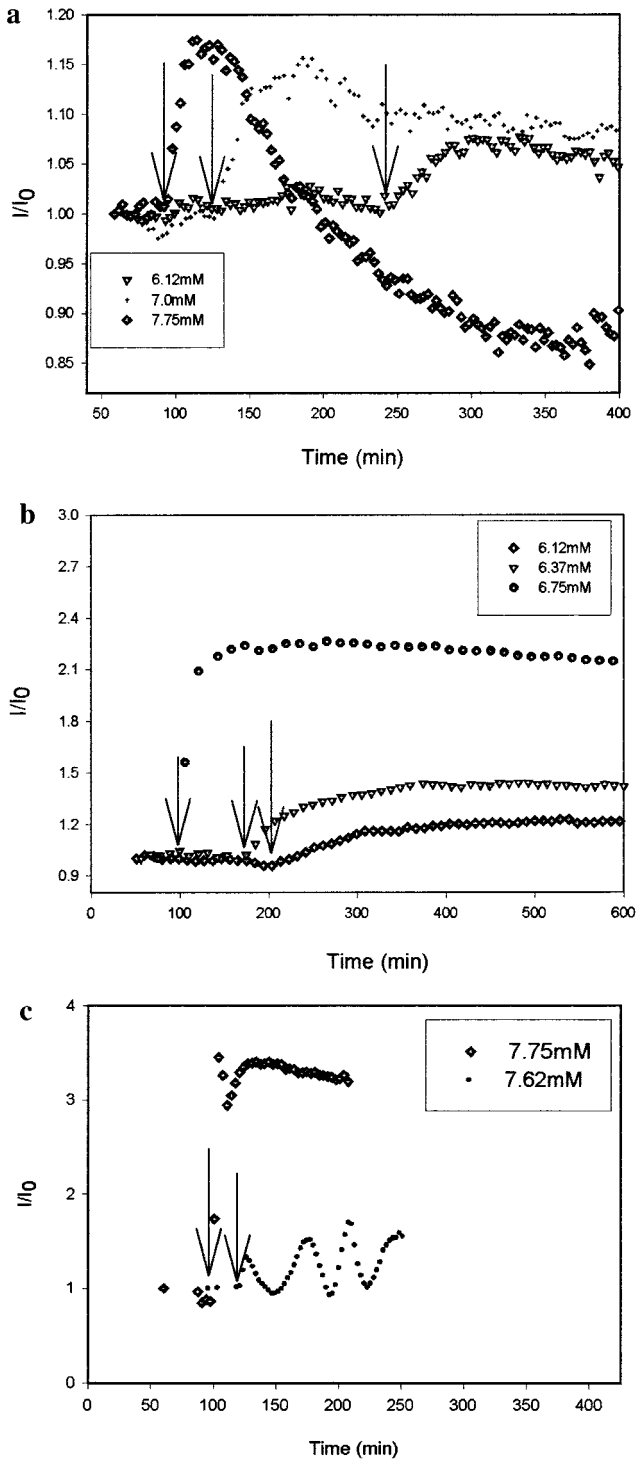

Figure 2. Evolution of the I/I_0 ratio versus time for different calcium/phosphate concentration. I_0 is the reflected intensity at the time zero at a given incidence angle, and I, the intensity at time t measured at the same incidence angle. (a) Signals measured on a PEI−(PSS−PAH)$_2$−PSS multilayer or on a bare silica surface. (b) Signals measured on a PEI−(PSS−PAH)$_2$ multilayer or (c) on a bare silica surface. Arrows on the figure represent the beginning of the nucleation process. The calcium/phosphate concentrations used are given in the inset with the corresponding symbols.

mated by the Debye−Hückel equation. The derivation of expressions 2−4 are given in appendix.

(15) Bates, R. G.; Acree, S. F. *J. Res. Natl. Bur. Stand. (U.S.)* **1943**, *30*, 129.

(16) *Handbook of Chemistry and Physics*, 67th ed.; CRC Press, Boca Raton, FL, 1986−1987; p D-163.

Table 3. Last Determined Thicknesses L (second column), and Induction Times (third column) for PEI−(PSS−PAH)$_2$−PSS and PEI−(PSS−PAH)$_2$ Films in Contact with Calcium/Phosphate Solutions at Different Concentrations (First Column)

conc (mM)	thicknesses (μm)	induction time (min)
	PEI−(PSS−PAH)$_2$−PSS	
5.00	/	/
5.75	0.25	240
6.12	0.25	250
7.00	0.55	129
7.75	0.85	95
	PEI−(PSS−PAH)$_2$	
4.50	/	/
5.75	/	/
6.12	2.0	206
6.37	2.2	182
6.75	3.7	117
6.75	3.7	102

We define the supersaturation ratio S_{OHAP} with respect to OHAP by:

$$S_{OHAP} = \left(\frac{IP_{OHAP}}{K_{SP/OHAP}}\right)^{1/9} \quad (5)$$

in which $K_{SP/OHAP} = 1.18\ 10^{-60}$ mol^9·L^{-9} [17] corresponds to the solubility product for OHAP, the ionic product IP_{OHAP} being evaluated at the onset of the nucleation process. Our evaluations of S_{OHAP} give 21 ± 1 for PEI−(PSS−PAH)$_2$ and 20 ± 1 for PEI−(PSS−PAH)$_2$−PSS. For comparison, in the absence of any seed, Nancollas and Mohan[18] could not observe any precipitation within 24 h for a Ca/P ratio of 1.6 in a solution at pH 7.4, T = 25 °C characterized by $S_{OHAP} = 25$. On the other hand, for the same Ca/P ratio, instantaneous nucleation was observed in the presence of salivary proteins for $S_{OHAP} = 4.1$.[19] On a bare silica surface, we observed the nucleation process of DCPD for a calcium/phosphate concentration corresponding to a supersaturation ratio relative to OHAP (S_{OHAP}) of 27. This shows that, *even if one does not form the same phase on bare silica and on multilayers, the polyelectrolyte multilayers exhibit a significant nucleating effect for calcium/phosphate crystals*.

By considering that, at the nucleation onset, the concentration of calcium and phosphate species are the same near the multilayer and in the solution, one can estimate, by means of relation 2 the interfacial pH (details can be found in the Appendix). The calculated pH values relative to the different surfaces and to the three inorganic phases (OHAP, DCPD, and OCP) are given in Table 2. It comes out that they are significantly lower than the pH value in the solution. Moreover the lowest pH value is found for OHAP indicating that at the interface supersaturation is highest with respect to OHAP since calcium and phosphate saturation concentrations are decreasing functions of the pH. However, according to literature, the calcium/phosphate phase which forms during the mineralization process depends on its relative supersaturation with respect to a particular inorganic phase, its ability to form nuclei and its growth rate. For relatively high supersaturation, for pH values not so far from neutrality, it was suggested that amorphous calcium phosphate (ACP) is normally first precipitated, ACP then converts into OHAP usually via OCP.[20] At intermediate

(17) Gramain, Ph.; Voegel, J. C.; Gumpper, M.; Thomann, J. M. *J. Colloid Interface Sci.* **1987**, *118*, 1934.

(18) Nancollas, G. H.; Mohan, M. S. *Arch. Oral Biol.* **1970**, *15*, 731.

(19) Campbell, A. A.; Nancollas, G. H. *Colloids Surf.* **1991**, *54*, 33.

(20) Elliot J. C. *Structure and Chemistry of the Apatites and Other Calcium Orthophosphates*; Elsevier Science B.V.: Amsterdam, 1994; p 155.

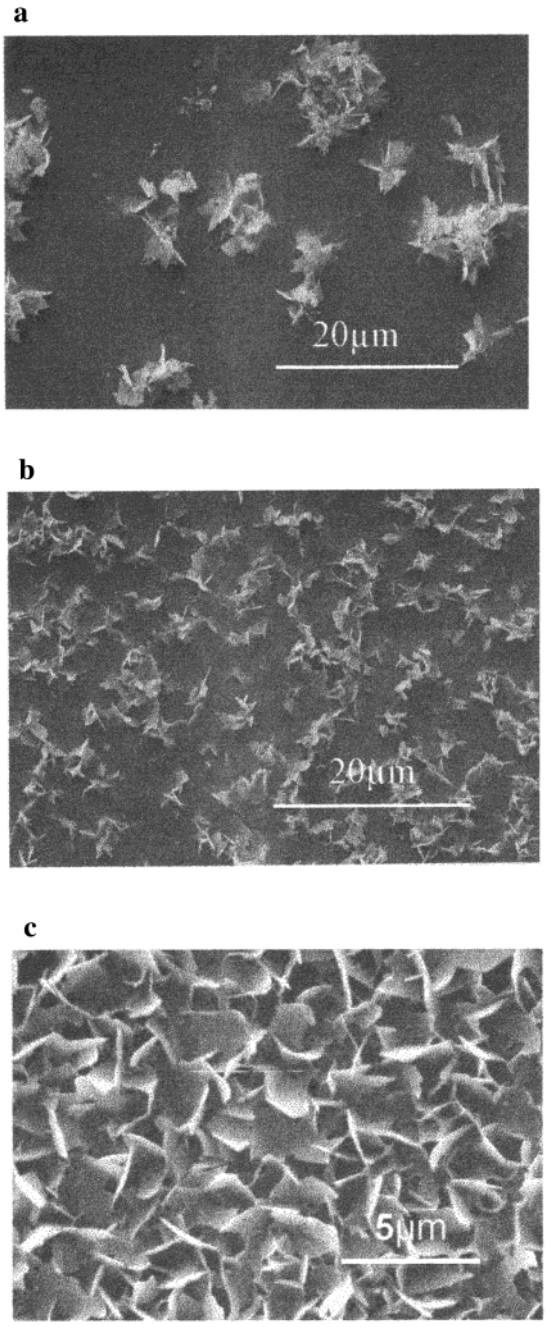

Figure 3. (a) SEM image of the silica surface coated with a PEI−(PSS−PAH)$_2$−PSS polyelectrolyte layer after its contact with a 6.75 mM of calcium/phosphate solution during 20 h. (b) SEM image of the silica surface coated with a PEI−(PSS−PAH)$_2$ polyelectrolyte layer after its contact with a 6.75 mM of calcium/phosphate solution during 20 h. (c) SEM image of the silica surface after a 20 h contact with a 7.62 mM calcium/phosphate solution.

supersaturation, the process seems to go via DCPD or OCP,[21] whereas direct formation of OHAP was reported at lower supersaturation.[22] The presence of OCP compatible with IR analysis is thus not unexpected.

Let us now analyze more quantitatively the dependence of the induction time on the supersaturation ratio. Classical nucleation theory[23] predicts that the induction time τ varies with

(21) van Kemenade, M. J. J. M.; de Bruyn, P. L. *J. Colloid Interface Sci.* **1987**, *118*, 564.

(22) Boskey, A. L.; Posner, A. S. *J. Phys. Chem.* **1976**, *80*, 40.

(23) Verdoes, D.; Kashchiev, D.; Rosmalen, G. H. *J. Cryst. Growth* **1992**, *118*, 401.

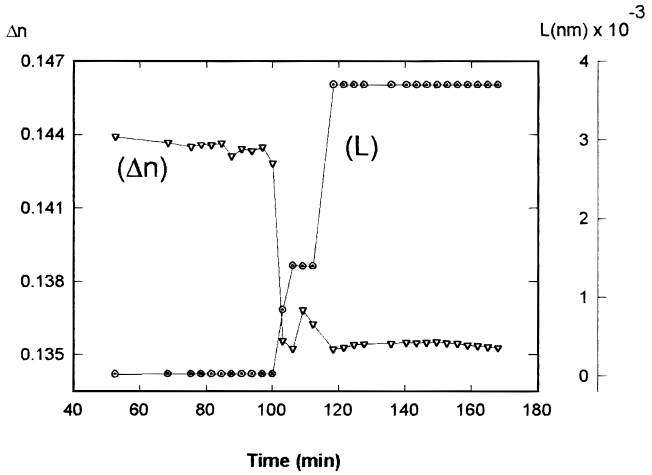

Figure 4. Evolution of the layer thickness L in nm (⊙) and the refractive index increment Δn (▽) for an experiment realized with a 6.75 mM calcium/phosphate solution in contact with a PEI−(PSS−PAH)$_2$ polyelectrolyte layer.

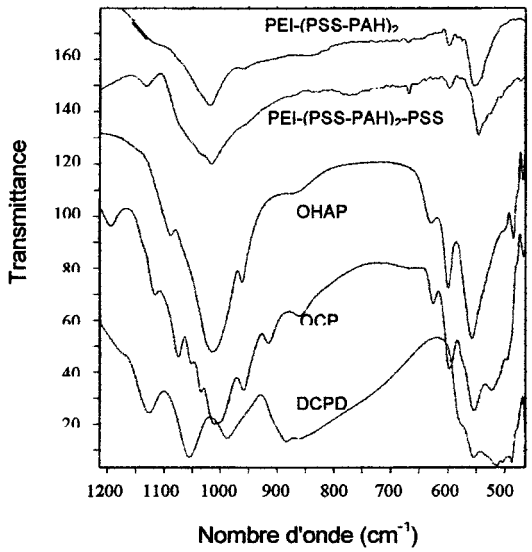

Figure 5. Infrared spectra of calcium/phosphate crystals formed on PEI−(PSS−PAH)$_2$, PEI−(PSS−PAH)$_2$−PSS polyelectrolyte multilayers and the spectra of pure OHAP, OCP, and DCPD samples. The origin of the different pure calcium/phospohate salts is indicated in the title of Table 4.

the S as:

$$\tau = A\frac{1}{(S-1)^{3/4}}\frac{1}{S^{1/4}}\exp\left(\frac{B}{4\ln^2 S}\right) \quad (6)$$

$$A = \left(\frac{3\alpha}{\pi K_J K_G^3}\right)^{3/4} \quad (7)$$

where A is practically an S-independent kinetic factor and

$$B = \beta\gamma^3\nu^2/(kT)^3\delta^2 \quad (8)$$

Here, β is a numerical shape factor (e.g., $16\pi/3$ for spheres), ν is the molecular volume, γ(J·m^{-2}) is the specific surface free energy (interfacial tension) characterizing the crystal/solution interface, and δ the number of ions in the formula unit. The induction time τ being, in first approximation close to $1/J(S)$,- we have plotted in Figure 6 $\ln\lfloor S^{1/4}(S-1)^{3/4}\tau\rfloor$ as a function of $1/\ln^2(S)$. Assuming a linear dependence between $\ln\lfloor S^{1/4}(S-1)^{3/4}\tau\rfloor$ and $1/\ln^2(S)$ one can estimate the value of an effective specific

Table 4. Principal Vibration Bands in cm^{-1} Obtained by IR Spectroscopy for OCP (kindly provided by Dr. Iijima, School of Dentistry, Asohi Univ., Japan), OHAP (Bio-Gel, HTP, Bio-Rad Lab., Richmond, CA), DCPD (Merck, catalog no. 2146, Darmstadt, Germany) and of the Calcium/Phosphate Salts Deposited onto PEI−(PSS−PAH)$_2$−PSS and PEI−(PSS−PAH)$_2$ Films (two last lines) in Contact with a 6.75 mM Calcium/Phosphate Solutions during 20 h[a]

OCP					1115				1051	1033	**1009**			957	914					860
OHAP						1088					**1014**		962					870		
DCPD	1175	**1128**							1056			**989**					**885**		**860**	
PEI−(PSS−PAH)$_2$−PSS							1073			1035	**1018**			950						
PEI−(PSS−PAH)$_2$							1073				**1018**			957						
OCP							**594**				**555**			523						
OHAP					627		**597**				**552**									
DCPD									557		552									
PEI−(PSS−PAH)$_2$−PSS		668					**598**				552		548	536		524		504		
PEI−(PSS−PAH)$_2$		660					**597**				552			536		524				

[a] Major peaks are indicated by bold-face characters.

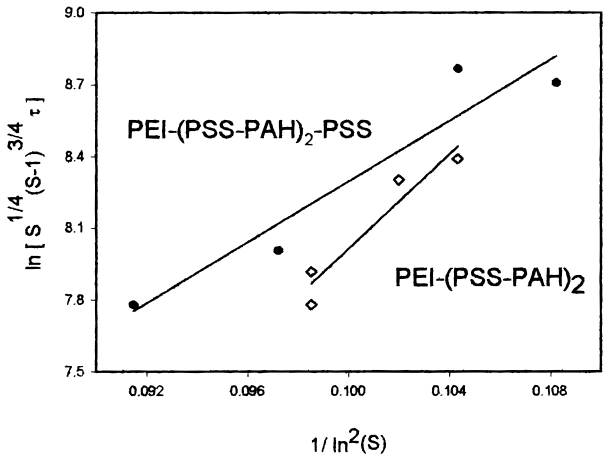

Figure 6. Plots of $\ln[S^{1/4}(S-1)^{3/4}\tau]$ versus $1/\ln^2(S)$ for PEI−(PSS−PAH)$_2$−PSS (●), and for PEI−(PSS−PAH)$_2$ (◇) brought in contact with calcium/phosphate solutions at different concentrations. Lines represent the linear regression for both systems.

surface free energy γ of 32 mJ·m^{-2} on PEI−(PSS−PAH)$_2$−PSS and of 37 mJ·m^{-2} on PEI−(PSS−PAH)$_2$. These values are, as expected, lower than the surface tensions determined for homogeneous nucleation of apatites (289 mJ·m^{-2} for fluorapatite,[24] and 87 mJ·m^{-2} for OHAP[25]). This seems to indicate that *the polyelectrolyte multilayers are very effective nucleating agents for calcium/phosphate crystals*. They can also be compared with the surface free energy of the overgrowth based on heterogeneous nucleation of OHAP on various substrates as 152 mJ·m^{-2} on DCPD,[26] 93 mJ·m^{-2} for OHAP,[27] 70 mJ·m^{-2} on collagen[28] 55 mJ·m^{-2} on phospholipids,[29] 90 mJ·m^{-2} on highly phosphorylated proteins,[30] and 92 mJ·m^{-2} for phosphorilated copolymers.[27] Our values of γ are thus smaller even if of the same order as the values of γ found on most of the surfaces.

By assuming that only charged sites near the last polymer layer are involved in the creation of nucleation sites, the effect of a negative polyelectrolyte film such as PEI−(PSS−PAH)$_2$−PSS on the calcium/phosphate nucleation process could be the consequence of a reduced H^+ counterions concentration close to the surface or to the strong calcium chelating properties of the negatively charged polyelectrolyte films. This subdivision of polyelectrolyte multilayers into charged interfacial zones and a quasi-neutral interior has been observed before.[13,31] Two similar explanations can be proposed for the effect of a positively charged multilayer such as PEI−(PSS−PAH)$_2$ which can either accumulate OH^- ions close to the surface or/and have strong phosphate chelating properties. One can also point out that in comparison to polymer films such as chitosan, the outer polyelectrolytes are quite more flexible and thus can change their conformations so that the positively (respectively, negatively) charge distributions can roughly fit with the negatively (respectively, positively) ionic group distributions of characteristic lattice planes of calcium/phosphate structures. Such an effect should be much more difficult to reach with rigid structures such as chitosan or with monolayers of adsorbed charged polymers

Conclusions

It was shown in this study that *polyelectrolyte multilayers, both negatively or positively charged, lead to a decrease of the supersaturating ratio for heterogeneous nucleation of calcium/phosphate crystals*, and this is, to the authors knowledge, the first time such a beneficial effect is observed on a positively charged surface (PEI−(PSS−PAH)$_2$ film). Moreover, it was found that the nature of the last layer has a pronounced influence on the crystal structure (no DCDP) and on the crystal morphology. Some mechanisms of action of the multilayers on the nucleation process were proposed on the basis of an increase of the concentration of some ions near the last polyelectrolyte layer of the multilayer. Further studies are however needed to support this view in which the amount and nature of chemical groups and surface charges are largely varied.

This study also constitutes a first step toward the design of new biomaterial coatings favoring osseointegration of implants in contact with hard biological tissues by increasing the ability of heterogeneous nucleation. This integration ability should be increased by additional adsorption of mineralization-inducting proteins or of small apatite crystals on these multilayers; such studies are currently under investigation.

Acknowledgment. We thank CNRS and INSERM for financial support through the program "Adhesion Cellules-Matériaux". This work was performed within the framework of the Research Network "Mécanismes physico-chimiques d'adhésion cellulaire: forces d'adhésion entre ligands et recep-

(24) Cappellen, P.; Berner, R. A. *Geochem. Cosmochem. Acta* **1991**, *55*, 1219.
(25) Arends, J.; Christoffersen, J.; Christoffersen, M. R.; Eckert, H.; Fowler, B. O.; Heughebaert, J. C.; Nancollas, G. H.; Yesinowski, J. P.; Zawacki, S. J. *J. Cryst. Growth* **1987**, *84*, 515.
(26) Koutsoukos, P. G.; Nancollas, G. H. *J. Cryst. Growth* **1981**, *53*, 10.
(27) Dallas, E.; Kallitsis, J. K.; Koutsoukos, P. G. *Langmuir* **1991**, *7*, 1822.
(28) Koutsoukos, P. G.; Nancollas, G. H. *Colloids Surf.* **1987**, *28*, 95.
(29) Dallas, E.; Ioannou, P. V.; Koutsoukos, P. G. *Langmuir* **1989**, *5*, 157.
(30) Saito, T.; Yamauchi, M.; Crenshaw, M. A. *J. Bone Miner. Res.* **1998**, *13*, 265.
(31) Schlenoff, J. B.; Ly, H.; Li, M. *J. Am. Chem. Soc.* **1998**, *120*, 7626.

teurs biologiques". The authors thank the Bruker for help in realizing the IR spectroscopic measurements.

Appendix

Detailed Calculation of the Ionic Products of OHAP, OCP, and DCPD Inorganic Phases. The ionic structures of OAHP, DCPD, and OCP correspond respectively to $Ca_5(PO_4)_3OH$ for OHAP, $CaHPO_4{\cdot}2H_2O$ for DCPD, $Ca_4H(PO_4)_3{\cdot}2.5H_2O$ for OCP, and their respective ionic products (IP) can be defined as:

$$IP_{OAHP} = \{Ca^{2+}\}^5\{PO_4^{3-}\}^3\{OH^-\} \quad (9)$$

$$IP_{DCPD} = \{Ca^{2+}\}\{HPO_4^{2-}\} \quad (10)$$

$$IP_{OCP} = \{Ca^{2+}\}^4\{PO_4^{3-}\}^3\{H^+\} \quad (11)$$

where the brackets correspond to the ionic activities. The same relations stand for the solubility products valid at equilibrium by replacing IP by K_{SP}. We used $K_{SP/OHAP} = 1.18\ 10^{-60}$ $mol^9{\cdot}L^{-9}$,[17] $K_{SP/DCPD} = 2.37\ 10^{-7} mol^2{\cdot}L^{-2}$,[32] $K_{SP/OCP} = 3.98\ 10^{-49}\ mol^8{\cdot}L^{-8}$.[32] Relations 9−11 can be derived by using the concentrations multiplied by the activity factors instead of the activities. The $f_{Ca^{2+}}$, $f_{HPO_4^{2-}}$, $f_{H_2PO_4^-}$, $f_{PO_4^{3-}}$ and f_{H^+} activity factors of Ca^{2+}, HPO_4^{2-}, $H_2PO_4^-$, PO_4^{3-}, and H^+ were evaluated from the extension of the Debye−Hückel law

$$\log(f_i) = -\frac{Az_i^2}{\mu^{1/2} + B{\cdot}a_i} \quad (12)$$

where μ is the ionic strength calculated by

$$\mu = \frac{1}{2}\sum_{i=1}^{n} C_i z_i^2 \quad (13)$$

C_i represents the concentration and z_i the number of charges of ions "i". A, B, and a_i are constants depending upon the temperature and on the dielectric constant of the solution. The values for a_i are: 6×10^{-8} cm for Ca^{2+}, 9×10^{-8} cm for H^+, and 4×10^{-8} cm for the different ionic phosphate forms.[33] A and B are respectively equal to 0.522 and 0.331×10^8 cm.[33]

The total phosphate concentration (P) can be expressed as a function of the calcium concentration since (Ca)/(P) = 1. However, P is constituted by the sum of four ionic species

$$[P] = [H_3PO_4] + [H_2PO_4^-] + [HPO_4^{2-}] + [PO_4^{3-}] \quad (14)$$

These ionics species are defined by three equilibrium relations

$$H_3PO_4 \leftrightarrow H^+ + H_2PO_4^- \quad (15)$$

$$H_2PO_4^- \leftrightarrow H^+ + HPO_4^{2-} \quad (16)$$

$$HPO_4^{2-} \leftrightarrow H^+ + PO_4^{3-} \quad (17)$$

and their equilibrium constants K_1, K_2, K_3 are: $K_1 = 6.53 \times 10^{-3}$ $mol{\cdot}L^{-1}$,[14] $K_2 = 6.57 \times 10^{-8}$ $mol{\cdot}L^{-1}$,[15] and $K_3 = 4.73 \times 10^{-13}$ $mol{\cdot}L^{-1}$.[16] K_1, K_2, K_3 are defined by:

$$K_1 = \frac{\{H^+\}\{H_2PO_4^-\}}{\{H_3PO_4\}} \quad (18)$$

$$K_2 = \frac{\{H^+\}\{H_2PO_4^{2-}\}}{\{H_2PO_4^-\}} \quad (19)$$

$$K_3 = \frac{\{H^+\}\{H_2PO_4^{3-}\}}{\{HPO_4^{2-}\}} \quad (20)$$

If one defines the fraction of phosphate ions present as PO_4^{3-} and HPO_4^{2-} by

$$F(PO_4^{3-}) = \lfloor PO_4^{3-} \rfloor / [P] \text{ and } F(HPO_4^{2-}) = \lfloor HPO_4^{2-} \rfloor / [P]$$

and combining these ratios with the definitions of the equilibrium contants K_1, K_2, K_3, one obtains

$$F(PO_4^{3-}) = \frac{K_1K_2K_3}{Q{\cdot}f_{PO_4^{3-}}} \quad (21)$$

with

$$Q = \{H^+\}^3 + \frac{K_1\{H^+\}^2}{f_{H_2PO_4^-}} + \frac{K_1K_2\{H^+\}}{f_{HPO_4^{2-}}} + \frac{K_1K_2K_3}{f_{PO_4^{3-}}} \quad (22)$$

Similarly, $F(HPO_4^{2-})$ the fraction of phosphate as HPO_4^{2-} can be defined by

$$F(HPO_4^{2-}) = \frac{K_1K_2\{H^+\}}{Q{\cdot}f_{HPO_4^{2-}}} \quad (23)$$

If one considers also the ionic product for water $K_w = 1.01\ 10^{-14}$ at 25 °C, then relations 9−11 can be expressed only versus $[Ca^{2+}]$ and $F(PO_4^{3-})$ for OHAP and OCP, or $[Ca^{2+}]$ and $F(HPO_4^{2-})$ for DCPD. One then derives relations 2−4 in which $F(PO_4^{3-})$ and $F(HPO_4^{2-})$ are only pH-dependent. From relations 2−4 when K_{SP} (the solubility products) are used instead of IP, it is possible to estimate from the experimental saturating calcium concentrations (C_c), the saturating pH values corresponding to OHAP, DCPD, and OCP (see Table 2).

Notation: {x} corresponds to the ionic activity of "x", and [x] to its concentration.

JA000783O

(32) Elliot, J. C. *Structure and Chemistry of the Apatites and Other Calcium Orthophosphates*; Elsevier Science B.V.: Amsterdam, 1994; p16.

(33) Moreno, E. C.; Gregory, T. M.; Brown, W. E. *J. Res. Natl. Bur. Stand. (U.S.)* **1966**, *70A*, 545.